Control strategy of wind turbine based on permanent magnet synchronous generator and energy storage for stand-alone systems

Deng, Fujin; Liu, Dong; Chen, Zhe; Su, Peng

Published in:
Chinese Journal of Electrical Engineering

DOI (link to publication from Publisher):
10.23919/CJEE.2017.7961322

Publication date:
2017

Document Version
Publisher's PDF, also known as Version of record

Control Strategy of Wind Turbine Based on Permanent Magnet Synchronous Generator and Energy Storage for Stand-Alone Systems

Fujin Deng[1] *, *Dong Liu*[2], *Zhe Chen*[2], *and Peng Su*[1]

(1. Department of Electrical Engineering, Southeast University, Nanjing, 210096, China;
2. Department of Energy Technology, Aalborg University, Aalborg, 9220, Denmark)

Abstract: This paper investigates a variable speed wind turbine based on permanent magnet synchronous generator and a full-scale power converter in a stand-alone system. An energy storage system(ESS) including battery and fuel cell-electrolyzer combination is connected to the DC link of the full-scale power converter through the power electronics interface. Wind is the primary power source of the system, the battery and FC-electrolyzer combination is used as a backup and a long-term storage system to provide or absorb power in the stand-alone system, respectively. In this paper, a control strategy is proposed for the operation of this variable speed wind turbine in a stand-alone system, where the generator-side converter and the ESS operate together to meet the demand of the loads. This control strategy is competent for supporting the variation of the loads or wind speed and limiting the DC-link voltage of the full-scale power converter in a small range. A simulation model of a variable speed wind turbine in a stand-alone system is developed using the simulation tool of PSCAD/EMTDC. The dynamic performance of the stand-alone wind turbine system and the proposed control strategy is assessed and emphasized with the simulation results.

Keywords: Variable speed wind turbine (VSWT), permanent magnet synchronous generator (PMSG), stand-alone system, energy storage system (ESS).

1 Introduction

Wind turbine technology has being undergoing a dramatic development and is now the world's fastest growing energy[1-4]. With large-scale exploration and integration of wind sources, variable speed wind turbine (VSWT) generator systems have become more popular than that of fixed speed[5-6]. Recently, the permanent magnet synchronous generator (PMSG) has received much attention in wind-energy application. The use of PM in the rotor of the PMSG makes it unnecessary to supply magnetizing current. Hence, for the same output, the PMSG will operate at a higher power factor because of the absence of the magnetizing current and will be more efficient than other machines. The multi-pole PMSG also improves significantly the reliability of the variable speed wind turbine by using a direct-drive train system instead of the gearbox, which also results in low cost[7-8].

Recently, trends make PMSG with a full-scale power converter structure more attractive for wind turbine[9]. VSWT with full-scale power converters present the distinct advantage that the converter decouples the generator from the grid. Hence, grid disturbances have no direct effect on the generator, which improves wind turbine performance[10]. Besides, the full-scale power converter not only offers a high degree of controllability over system variables, it is also particularly suited to incorporation and control of electrical energy storage capacity.

In normal grid-connected operation with the aforementioned full-scale power converter structure, when wind power is a relatively small portion of a strong grid, the grid-side converter is used to regulate the DC-link voltage while the generator-side converter regulates the generator to achieve the desired power transfer[11-12]. On the other hand, in the case of operation in a weak grid, when wind power becomes a significant portion of the power system or even the sole energy source, the wind turbine is expected to maintain the grid-side voltage and frequency. The weak-grid condition can be a result of intentional separation or islanding from the grid or grid faults. It applies as well to the stand-alone operating mode. For a stand-alone system, the output voltage of the load-side converter has to be controlled in terms of amplitude and frequency, while the DC-link voltage would be controlled from the generator-side converter. A hybrid adaptive control algorithm is proposed in [13] and [14] that search for the optimal PMSG acceleration to achieve the maximum wind generator power change rate to match the load power variation. In [13] and [14], the DC-link voltage is indirectly regulated by controlling the PMSG speed variation to regulate the captured power by generator. Nevertheless, there are some drawbacks for this proposed algorithm. The effectiveness of the control, measured by how fast the captured wind power can be adjusted through the PMG speed control to match the load power variation, depends primarily on the characteristics of wind power versus turbine/generator speed, the system mechanical inertia, as well as the DC-link capacitor. As a result, in case of the large variation of the load power, there would be a large fluctuation for the DC-link voltage, which may affect the performance of the wind turbine and even damage the power

* Corresponding Author, E-mail: fde@et.aau.dk.

electronics equipment. Reference [7-8] presented a novel control strategy for a variable-speed wind turbine with a PMSG in a stand-alone system, where the load-side inverter is used to regulate the DC-link voltage, output voltage, and frequency. The generator-side converter is adopted to track the optimal energy from the wind. Here, the excess power during fault or over generation is dissipated by the dump-resistor and stored by the energy storage system. It means that the dump-resistor would continuously work in the stand-alone system if the load power is less than the optimal power and the energy storage system is full, which may be not practical. The Takagi-Sugeno fuzzy approach was applied to the VSWT in a stand-alone system to improve system performance[15].

Batteries are the most popular storage system. As far as their application range is concerned, battery energy storage systems (BESS) show almost no restrictions. While the BESS possesses higher energy capacity than several other energy storage media, and hence, is suitable for the long-term load-tracking operation[16-17], BESS is also shown to be cost-effective for use in power system[18-19]. Fuel cells (FCs) also show great potential to be green power sources of the future because of the many merits they have, such as high efficiency, zero or low emission of pollutant gases, and flexible modular structure[20].

This paper incorporated ESS including BESS and FCs with a VSWT based on PMSG, full-scale power converter in a stand-alone system. The generator is indirectly connected to the load through the full-scale power converter, which is composed of a generator-side AC/DC converter, DC-link capacitor, and grid-side DC/AC inverter. The ESS is connected to the DC link of the power converter. In this paper, an efficient control strategy for a stand-alone VSWT conversion system is developed, where the wind turbine system is able to fast supply the load and wind speed variation, and keep the load-side voltage amplitude and frequency. The fluctuation of the voltage on the DC-link capacitor could be limited in a small range.

This paper is organized as below. Section 2 investigates the basic design issues, such as system configuration, wind turbine size, ESS power and the storage capacity needed to support the intermittent power output and so on. Section 3 introduces the model of the VSWT system. In Section 4, a control strategy is proposed for this wind turbine in a stand-alone system, which is able to fast regulate the captured wind power to match the loads variation. The fluctuation of the DC-link voltage because of the wind speed change or load variation could be limited in a small range. Section 5 validates the proposed control with simulation. A model for variable speed direct-drive PMSG wind energy conversion and ESS in a stand-alone generation system is simulated and carried out with the PSCAD/EMTDC.

2 System configuration and sizing

2.1 System configuration

Fig.1 shows the stand-alone system configuration, where the renewable wind power is taken as the primary source while the ESS is used as a backup and storage system. A direct-drive PMSG is used as a wind turbine generator, whose capacity is discussed later. The PMSG is connected to the variable loads through the electric power converter and a step-up transformer. The electric power converter is composed of AC-DC-AC converter/inverter, which could make the PMSG operate at variable speed by the generator- side AC/DC converter, and also supply the constant frequency output to the power system through the load-side DC/AC inverter. The ESS is used to address the intermittent behavior of renewable energy sources in this stand-alone system, which is integrated with the full-scale power converter and connected at the DC-link bus through bi-directional DC/DC converter interfacing circuits.

2.2 Wind turbine and energy storage system

Fig.1 shows the use of ESS to compensate for the intermittent power output of the wind turbine in a stand-alone system. To illustrate the performance, the actual load profile and wind power production in an area in Denmark, reported in [21], are considered, which are shown in Fig.2.

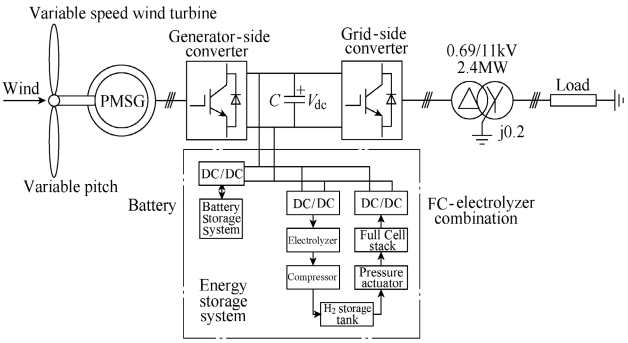

Fig.1 Block diagram of a VSWT based on direct-drive PMSG, full-scale power converter and ESS in a stand-alone system

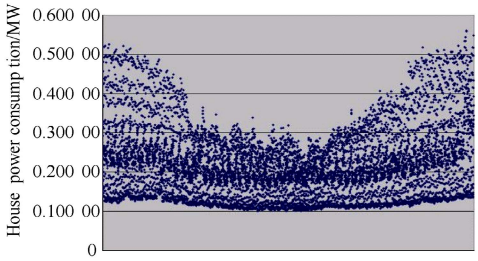

(a) House power consumption in 2007

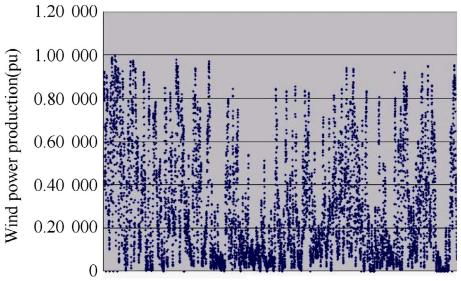

(b) Wind power production in 2007

Fig.2 Load profile and wind power production in Denmark[21]

A few kinds of wind turbine with different sizes are considered. Fig.3 shows the energy required for these different wind turbines. Assuming that the ESS is ideal, i.e., it can store this required energy without power capacity limit, this figure indicates that the required energy peak value appears in December because of the low wind power production in December as shown in Fig.2, which is almost a few times higher than the required energy in the other months.

In this article a fuel-cell-battery hybrid is adopted as the ESS shown in Fig.1. Owing to the main weak points of FC such as its slow dynamics dominated by temperature and fuel-delivery system, the fast load or wind power production variations may cause a high voltage fluctuation. Hence, a system powered solely by FC is not economical. The battery is used here together with a FC to construct a fuel-cell-battery hybrid power source, which can improve the performance of the wind turbine system[22].

In this study, a small capacity battery energy storage system and a big capacity FC are adopted. The small energy intermittence during the first eleven months could be compensated by a small capacity battery, which has high energy efficiency as 80%. The combination of FC and BESS could provide the huge energy deficit in the last month. As well, more energy could be collected by the big capacity FC-electrolyzer combination all the year round and transformed to hydrogen, which could be supported to the customers in normal life.

The integration of an appropriate wind turbine and the related ESS could minimize the overall costs in the stand-alone system. Consequently, the design of this stand-alone system is to determine the wind turbine capacity, the ESS capacity and power based on a cost-benefit analysis.

The total investment cost of this stand-alone system is a combination of the wind turbine cost and ESS cost. Normally, the wind turbine cost is around 1 k€/kW. The ESS cost contains initial installation cost and the corresponding maintenance and operational cost. The cost of the ESS (Battery and FC) is primarily determined by the storage capacity and the power conversion system's nominal power, which may be calculated below[23].

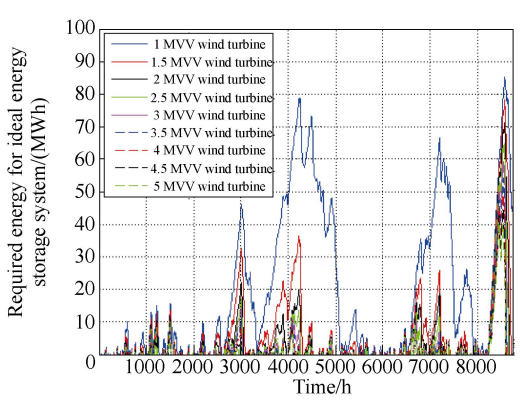

Fig.3 Energy required for ideal energy storage system

$$C_{ss} = IC_{ss} + \mathrm{MOC}_{ss} = (c_e E_{ss} + c_p N_{ss})(1+m) \quad (1)$$

where C_{ss} is the total cost of the ESS. IC_{ss} is the initial installation cost. MOC_{ss} is the maintenance and operation cost. c_e and c_p are the specific power cost coefficient related to the storage capacity and the nominal power of the conversion. N_{ss} is the nominal power of the conversion. m is the ratio of the maintenance and operation in the initial capital investment. E_{ss} is the practical storage capacity, which may be estimated by the following relationship[23]:

$$E_{SS\_BE} = \frac{E_{B\_ideal}}{\mathrm{DOD}\cdot\eta_b} \quad (2)$$

$$E_{SS\_FC} = \frac{E_{FC\_ideal}}{\eta_{fc}} \quad (3)$$

where E_{B_ideal} and E_{FC_ideal} are the required ideal capacity of battery and FC respectively. DOD is the maximum depth of discharge of battery. η_b and η_{fc} are energy efficiency of battery and fuel cell respectively. These parameters are given in the Appendix, which is derived from[23].

Fig.2 shows the peak load demand as 0.51 MW during the first eleven months. Hence, the size of BESS should be more than or equal to 0.6 MW, with the power efficiency of the battery as 85%. The peak load demand in the last month is shown as 0.55 MW in Fig.2. Thus, the nominal power of the FC-electrolyzer combination should be more than or equal to 0.79 MW, with the power efficiency as 70%. In this study, the maximum input power and the nominal output power of the ESS is assumed to be the same.

Normally, the energy capacity of the ESS is limited by its power capacity during operation. With the different power capacity of BESS, the required energy for the same wind turbine may be different. Based on the data of the energy consumption and wind power production in Fig.2 and the ESS cost demonstrated by (1)~(3), the optimal ESS power and energy capacity for different wind turbine sizes are obtained to minimize the costs, which are listed in Table 1. The total costs for the different wind turbine sizes is also given and listed in Table 1. It is clear that the 4MW wind turbine system is selected because of the minimal cost, where the battery and FC are 16.7MWh and 100MWh respectively.

This paper's interest is focused on the operational principle of the VSWT in a stand-alone system, where the BESS is used to supply transient power under the variation of loads or wind power production, so as to keep the DC-link voltage fluctuation in a small range. The basic components of the wind turbine system, the operational principle, the realization of the simulation and the validated results will be presented in the following sections.

3 Wind turbine model

The VSWT system in Fig.1 is a complex electromechanical system. The model of the system is developed in the dedicated power system analysis tool PSCAD/EMTDC.

Table 1 Characteristic of wind turbine and energy storage system

WT/ MW	BESS			FC			Cost			
	Power/ (MWh) efficiency (85%)	Ideal capacity E_{BE_ideal}/ (MWh)	Capacity E_{SS_BE}/(MWh) DOD (65%) & efficiency (80%)	power (MW) efficiency (70%)	Ideal capacity E_{FC_ideal}/ (MWh)	Capacity E_{SS_FC}/(MWh) efficiency (45%)	WT/ (k€)	BESS/ (k€)	FC/ (k€)	Total/ (k€)
1.0	0.65	78.7	151.3	0.79	6.5	16.0	1000	31867	269	33136
1.5	0.67	36.3	69.8	0.79	41.8	103.2	1500	14744	443	16687
2.0	0.6	22.1	42.5	0.79	49.2	121.5	2000	9009	480	11489
2.5	0.6	17.2	33.1	0.79	47.5	117.3	2500	7030	472	10002
3.0	0.6	14.2	27.3	0.79	44.9	110.9	3000	5819	459	9277
3.5	0.6	11.2	21.5	0.79	43.0	106.2	3500	4607	449	8556
4.0	0.6	8.7	16.7	0.79	40.5	100.0	4000	3598	437	8035
4.5	0.6	7.6	14.6	0.79	37.0	91.4	4500	3153	420	8073
5.0	0.6	7.2	13.8	0.79	33.7	83.2	5000	2992	403	8395

3.1 Aerodynamic model

The mechanical power extracted from the wind can be expressed as follows[24],

$$P_{\mathrm{w}} = \frac{1}{2}\rho\pi R^2 v^3 C_{\mathrm{p}}(\theta,\lambda) \tag{4}$$

where P_{w} is extracted power from the wind, ρ is the air density (kg/m^3), R is the blade radius (m), v is the wind speed(m/s) and C_{p} is the power coefficient which is a function of the pitch angle of rotor blades θ(deg) and of the tip speed ratio λ. The term λ is defined as $\lambda = \omega_{\mathrm{w}}R/v$, with ω_{w} the wind turbine speed.

The power coefficient may be calculated as

$$C_{\mathrm{p}} = 0.73\left(\frac{151}{\lambda_i} - 0.58\theta - 0.002\theta^{2.14} - 13.2\right)\cdot \mathrm{e}^{-18.4/\lambda_i} \tag{5}$$

with

$$\frac{1}{\lambda_i} = \frac{1}{\lambda - 0.02\theta} - \frac{0.003}{\theta^3 + 1} \tag{6}$$

Based on (1)~(3), the relation between the optimal power and the wind turbine speed can be obtained below.

$$P_{\mathrm{w\_max}} = \frac{1}{2}\rho\pi R^5 \frac{C_{\mathrm{p\_max}}}{\lambda_{\mathrm{opt}}^3}\cdot\omega_{\mathrm{w}}^3 \tag{7}$$

In the variable speed wind turbine operation, the generated active power depends on the power coefficient C_{p}, which is related to the portion of power extracted from the wind. For each wind speed, there exists a specific point in the wind turbine output power versus rotating-speed characteristic where the output active power is maximized. During the period of high wind speed, the variable-pitch control system would act to make the wind turbine operate at the rated power[25-28]. In this paper, the pitch angle control system could be modeled referring to [29-30], which is not detailed here.

3.2 Mechanical drive train

According to [31-32], under a comparative study of wind turbine generator system using different drive train models, it has been shown that the two-mass model in Fig.4 is suitable for transient stability analysis. The mode of two-mass drive train is described below[1, 30].

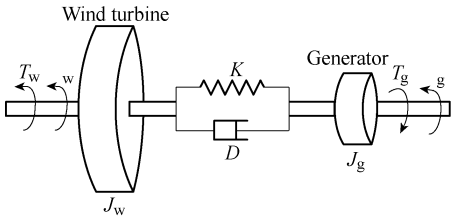

Fig.4 Block diagram of the two-mass model.

$$\begin{cases} J_{\mathrm{w}}\dfrac{\mathrm{d}\omega_{\mathrm{w}}}{\mathrm{d}t} = T_{\mathrm{w}} - K\theta_{\mathrm{wg}} - D(\omega_{\mathrm{w}} - \omega_{\mathrm{r}}) \\ J_{\mathrm{g}}\dfrac{\mathrm{d}\omega_{\mathrm{r}}}{\mathrm{d}t} = K\theta_{\mathrm{wg}} + D(\omega_{\mathrm{w}} - \omega_{\mathrm{r}}) - T_{\mathrm{g}} \end{cases} \tag{8}$$

where J_{w} and J_{g} are the equivalent wind turbine inertia and generator inertia respectively. Torque T_{w} and T_{g} represent the aerodynamic torque of the wind turbine and the generator loading torque, respectively. ω_{w} and ω_{r} are the wind turbine and generator rotor speed respectively. θ_{wg} is the angle between the turbine rotor and the generator rotor. K is the elastic characteristic of the shaft. D is the mutual damping between the two masses.

3.3 Full-scale power converter

A PMSG model available in the software package PSCAD/EMTDC is used here, which is controlled by the full-scale power converter. This power converter is composed of the generator-side AC/DC converter, DC-link capacitor, and the load-side DC/AC inverter. Each of converter/inverter is a standard 3-phase two-level unit, composed of six IGBTs and antiparallel diodes.

3.4 Battery energy storage system

The schematic diagram of BESS is shown in Fig.5(a), which is composed of a DC-DC buck/boost converter and a battery model. The battery is considered to be connected to the DC link of the full-scale power converter through the DC/DC converter as the ESS. In this study, a third-order equivalent battery circuit model developed by Ceraolo[33-34] is considered for accurate representation of battery charge/discharge characteristics and estimating the SOC of the battery. The model has been reproduced in Fig.5(b). In this model, the main branch including E_{m}, R_1, C_1, and R_2

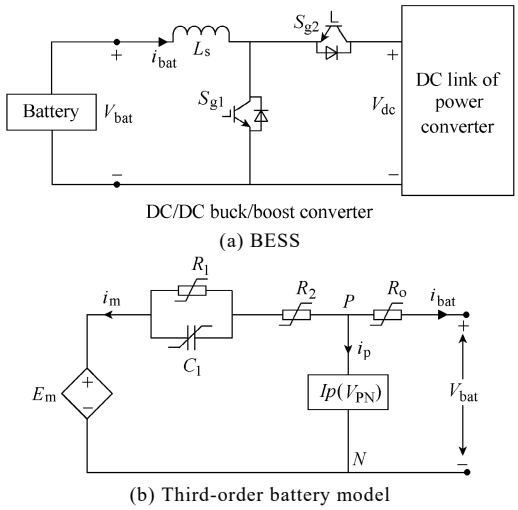

Fig.5 Block diagram

approximates the battery charge/discharge dynamics. The *PN* parasitic branch accounts for the self-discharge, and R_0 approximates the overcharge resistance. As the figure indicates, the resistive and capacitive elements are nonlinear and current-dependent, which can be determined empirically[35-36].

4 Principle of operation

In this stand-alone wind generation system, which is composed of PMSG, BESS and full-scale power converter, the DC-link voltage of power converter is kept constant by BESS. The amplitude and frequency of the load-side voltage are controlled by the load-side converter. The generator-side converter is used to supply the demanded power. The detailed operational principles of the wind turbine system are depicted below.

4.1 Control of energy storage system

The ESS here is only considered as BESS which has the bi-directional power control ability. It is used to keep the DC-link voltage V_{dc} of the power converter constant as 2.5 kV. The BESS has the ability to provide or absorb power in the DC link of the full-scale power converter. If the DC-link voltage V_{dc} is over the reference value V_{dc_ref}, the BESS would absorb energy from the DC link and reduce the voltage V_{dc} to V_{dc_ref}. Here, the battery is charged. Once the DC-link voltage is less than the reference value, the energy would be injected into the DC link so as to increase the voltage V_{dc} to V_{dc_ref} by discharging the battery.

Such a BESS is built with lead-acid batteries, by taking the individual units in series and parallel to get the desired voltage and energy rating. In this study, the BESS energy and power capacity is 16.7MWh and 0.6MW respectively, and the voltage V_{bat} is selected as 2kV. As the battery cell rated voltage is 2.135V and capacity C_{10} is 500Ah, one BESS branch is to consist of 937 cells, connected in series. 17 of these series strings are in parallel to obtain the desired energy and power rating. The battery parameters are given in the Appendix, which were taken from [34].

As for the battery, one important issue is the state of the charge (SOC). The BESS model in Fig.5 is used to estimate the SOC by using the procedure proposed in [34]. As it is not desired to deplete or overcharge the battery, the SOC of the battery should be kept within proper limit (i.e., between 35% and 100% in this paper) and needs to be determined accurately for the controller operation. When the SOC is measured less than 35% or more than 100%, the battery will stop discharging or charging controlled by power electronics interface.

Based on the above analysis, a simple control block for the BESS has been developed, as shown in Fig.6, where a DC-link voltage controller is used here to regulate the DC-link voltage of the full-scale power converter. The boost converter and buck converter with 1kHz switching frequency are controlled by two current controller branches in discharging and charging situations, respectively. The two converters could not conduct simultaneously. The logic table is described in Fig.6, where the switch signals between the two converters is not only based on the DC-link voltage V_{dc}, but also the measured battery current i_{bat}, as shown in Fig.5.

4.2 Control of generator-side converter

The generator-side converter connected to the stator of the PMSG effectively decouples the generator from the load, which is used to continuously deliver the energy from the generator to the DC link. The generator output power P_g should meet the power demand P_{sum}, which is the summation of the load power requirement P_{load} and the battery power requirement P_{bess}. It can be directly achieved through the regulation of the generator-side converter.

Considering the wind turbine characteristic in the Appendix and the maximum power point tracking (MPPT) method[28], the rotor speed versus power characteristic that leads to optimal energy capture is developed shown as Fig.7. Here, for the MPPT operation, rotor speed is used as a controller input instead of wind speed, because the rotor speed can be measured more precisely and more easily than the wind speed. In order to avoid large power fluctuations when rotor speed changes near the minimum rotor speed, a control characteristic similar to that leads to optimal energy capture are adopted[37]. The control characteristic is depicted by the curves *AB* in Fig.7.

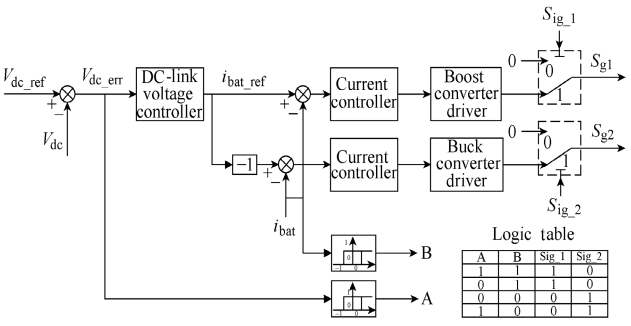

Fig.6 Schematic diagram of the control structure for the BESS

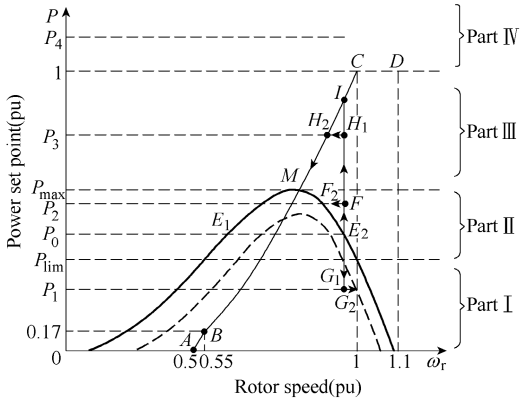

Fig.7 Optimal rotor speed versus power characteristic

For a given power demand P_0 in Fig.7, there would be two possible operation points (e.g. E_1 and E_2) for the generator operation (the power converter loss is neglected). Based on the torque versus rotor speed characteristic, the point E_2 is the steady operation point. Actually, in this operational principle, the wind turbine steady operation points are located at the right side of the optimal power curve (including the optimal power curve). For a power versus rotor speed characteristic corresponding to a given wind speed, there may be four operation parts including I, II, III and IV, for the stand-alone wind turbine system.

Part I: power demand is below P_{lim}, where the rotor speed ω_r reaches the upper limit in this situation, as shown in Fig.7. In this area, the variable-pitch control is active to change the characteristic curve from solid line to dash line to limit the rotor speed ω_r. When the power demand drops from P_0 to P_1, the generator would instantaneously supply the demanded power through the regulation of the generator-side converter. The PMSG works from point E_2 to G_1, and then straightly to G_2.

Part II: power demand is between P_{lim} and the maximum power P_{max}. When the demanded power stepped from P_0 to P_2, the generator power would immediately jump from point E_2 to F_1 to meet the requirement. At last, the wind turbine works steadily at point F_2.

Part III: power demand is between P_{max} and the rated power. When the demanded power is increased from power P_0 to P_3, the generator power is controlled by the generator-side converter to point H_1 and then goes straight towards to point H_2. Afterwards, the wind turbine operates along with the optimal power curve, to the maximum power point M.

Part IV: power demand is above the rated power. When the demanded power is stepped up from P_0 to a high value which is over the rated power, the wind turbine would jump from E_2 to I, and then operate toward to the maximum power point M along with the optimal power curve.

Based on above analysis, the proposed control strategy for the generator-side converter has been developed in this paper, as shown in Fig.8. As to the given wind turbine speed ω_w, if its corresponding optimal power P_{opt} is more than or equal to the demanded power P_{sum}, the generator power reference

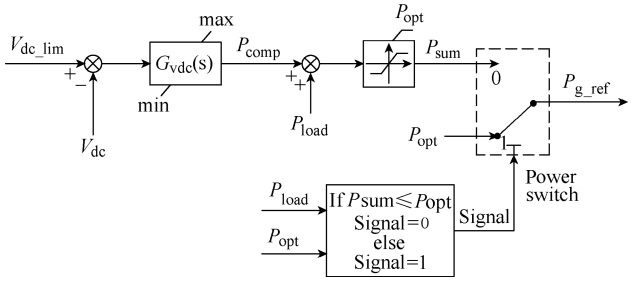

Fig.8 Block diagram of the proposed control strategy for the generator-side converter

is set as the power P_{sum}, which is the sum of the load power P_{load} and the power compensation component P_{comp}. Here, the compensation P_{comp} is used to charge the battery. On the other hand, when the demanded power is more than the optimal power, the PMSG is operated following the optimal power P_{opt}.

The power storage regulation could be realized through a voltage regulator $G_{\text{vdc}}(s)$ with the upper limit as 0.6MW, which is the nominal power of the BESS. Normally, in order to capture the maximum energy for BESS, the compensation P_{comp} is given as 0.6MW, which is the maximum power capacity of BESS. It means that the BESS may lose functionality to reduce the DC-link voltage if the overvoltage appears in the DC link, because the BESS can not absorb more energy. Here, the voltage regulator $G_{\text{vdc}}(s)$ starts to reduce the compensation P_{comp} to keep the DC-link voltage if the V_{dc} is over $V_{\text{dc\_lim}}$, which is set as 1.1 per unit.

The power regulation by the generator-side converter can be realized through the control structure shown in Fig.9. The controller is based on the dynamic model of the PMSG in the synchronous rotating frame (9), with the d-axis is aligned with the rotor flux[13].

$$\begin{cases} u_{ds} = R_s i_{ds} + L_d \dfrac{\mathrm{d}i_{ds}}{\mathrm{d}t} - L_q \omega_r i_{qs} \\ u_{qs} = R_s i_{qs} + L_q \dfrac{\mathrm{d}i_{qs}}{\mathrm{d}t} + L_d \omega_r i_{ds} + \omega_r \psi_r \end{cases} \tag{9}$$

where u_{ds} and u_{qs}, i_{ds} and i_{qs}, L_d and L_q are the d- and q-components of the stator voltage, of the stator current and of the stator inductance, respectively. R_s, ψ_r and ω_r stand for stator resistance, permanent magnet flux and rotor speed, respectively.

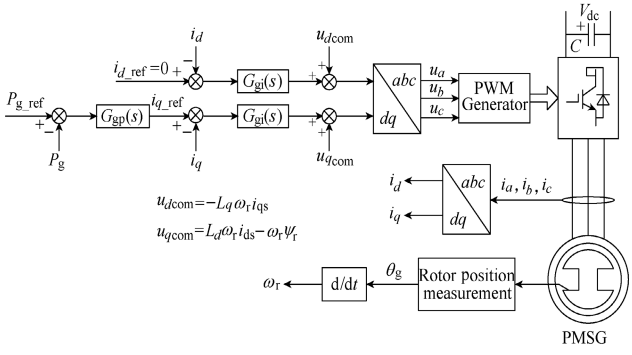

Fig.9 Block diagram of the control structure for generator-side converter

As the converter is directly connected to the PMSG, its q-axis current is proportional to the active power. The d-axis stator current is proportional to the reactive power. The reactive power reference is set to zero to perform unity power factor operation.

In Fig.9, the control block for the generator-side converter adopts double control loops. A power controller $G_{gp}(s)$ is used in the outside loop to regulate the generator power P_g, and produces corresponding q-axis current command i_{q_ref}. In inside loop, the current controllers are adopted to regulate d- and q-axis stator current to track the command value.

4.3 Control of load-side inverter

The objective of the load-side inverter is to regulate the output voltage, which has to be controlled in terms of amplitude and frequency as no grid exists in a stand-alone system. Vector control technique has been developed for the load side inverter as shown in Fig.10. The controllers are based on the dynamic model of the voltage source converter in the synchronous rotating frame (10) with the rotating frequency as 50 Hz, where u_d, u_q, i_d, i_q are the load-side voltages and currents in d, q reference frame. The double control loop structure is adopted here. The inside loop is used to control the load-side current. The outside loop is used to maintain the output voltage amplitude.

$$\begin{cases} u_d = u'_d + R_f i_d + L_f \dfrac{\mathrm{d}i_d}{\mathrm{d}t} - \omega L_f i_q \\ u_q = u'_q + R_f i_q + L_f \dfrac{\mathrm{d}i_q}{\mathrm{d}t} + \omega L_f i_d \end{cases} \tag{10}$$

where L_f, R_f and ω are filter inductance, resistance and angular speed, respectively.

In the generator-side converter and the load-side converter, the triangular carrier signal is used as the carrier wave of PWM operation. The carrier frequencies are both selected as 1kHz. In addition, these controllers in the BESS, generator-side converter and load-side inverter are all simple proportional-integral (PI) controllers. Combining the parameters in the Appendix, these PI controllers have been designed with the frequency-response design method referring to [38], and the results are given in the Appendix.

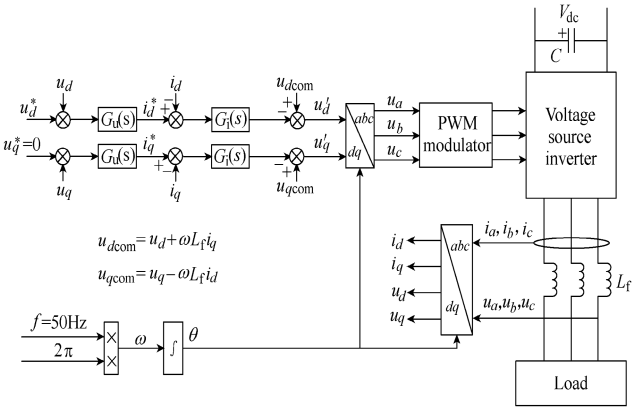

Fig.10 Block diagram of the voltage and frequency control for load-side converter

5 Simulation based verification

A 4MW VSWT in a stand-alone system is modeled as shown in Fig.1, which is built with the models in section III. The initial SOC of the BESS is set as 60%. The system parameters are given in the Appendix. The proposed operational principle for the wind turbine system is tested with different loads, as well as the variable wind speed. In the first case, the performance of the wind turbine is verified at the fixed wind speed under different loads. In the second case, the performance of the wind turbine is tested at constant loads under the variable wind speed. In the third case, the stand-alone system capability is demonstrated at variable wind speed and loads.

5.1 The first case

In the first case, a constant wind speed as 10 m/s is adopted. Fig.11 shows the response of the system for a step change of load power from 0.47 per unit to 0.75 per unit at 40s, and then to 0.3 per unit at 100s.

Initially, the PMSG is operated along with P_{sum}, which is less than P_{opt}. The BESS absorbed the energy with the maximum power as 0.6 MW shown in Fig.11(f). When loads power stepped up at 40s, generator torque increased quickly to make that the generator power track the load power change, which results in that the optimal power in Fig.11(h) decreases along with the reduction of the wind turbine speed. Meanwhile, the dashed line optimal power P_{opt} is less than the sum power P_{sum}. Based on Fig.8, the generator power is switched to track the optimal power. Here, the generator power is not enough to support the loads. The BESS starts to provide the loads together with the generator shown in Fig.11(f), and keep the DC-link voltage constant. Owing to energy release, the SOC of the battery is reduced as shown in Fig.11(g).

Since 100s, the sum power P_{sum} is stepped down and less than power P_{opt} because of the decrease of the loads. The generator starts to work along with P_{sum} again, and the BESS absorb the maximum power as 0.6 MW from the wind turbine shown in Fig.11(f). Along with the charge, the SOC is increased again as shown in Fig.11(g). During the sudden decrease of loads, the BESS could not absorb the power fast enough, which results in the DC link overvoltage. In order to keep the DC link voltage, the compensation P_{comp} is reduced at 100s shown in Fig.11(h) so as to reduce the generator power. Here, the fluctuation of DC-link voltage is only 0.11p.u., shown in Fig.11(e). Owing to the decrease of the generator power, the wind turbine speed is increased as shown in Fig.11(b), which causes the action of the pitch angle control system, shown in Fig.11(c).

5.2 The second case

The second case shows the performance of the system for a step change of wind speed from 10m/s to 8m/s at 40s, and then to 11.5m/s at 100s. Here, the loads power is constant as 0.47 per unit.

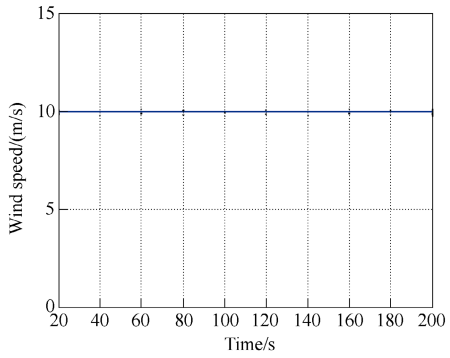

(a) Wind speed

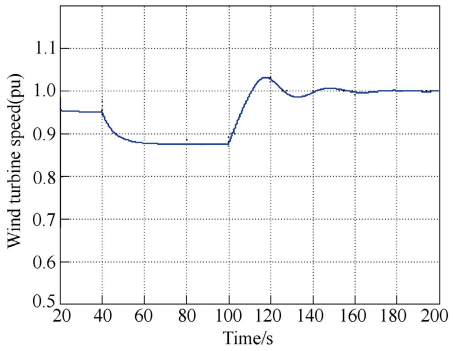

(b) Wind turbine speed

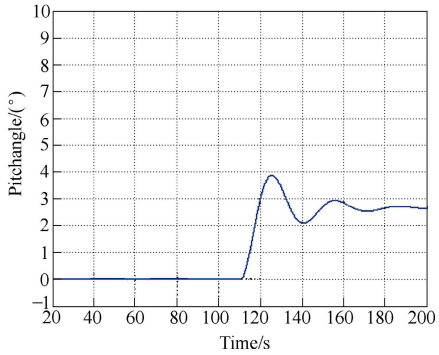

(c) Pitch angle

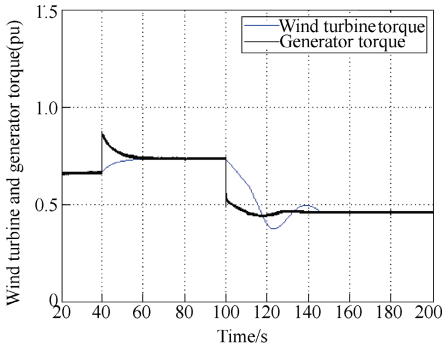

(d) Wind turbine torque and generator torque

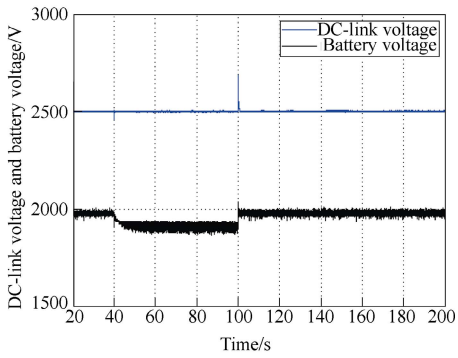

(e) DC-link voltage and battery voltage

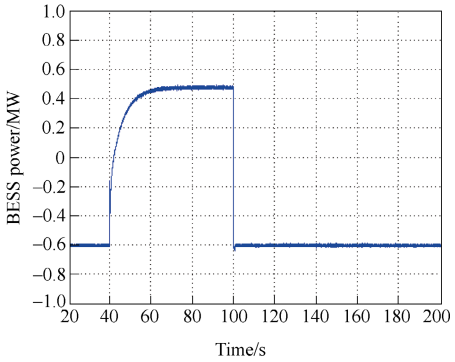

(f) BESS power

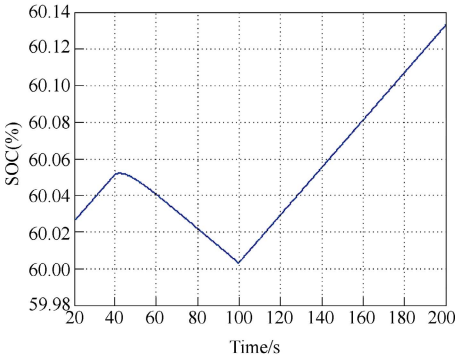

(g) SOC of battery

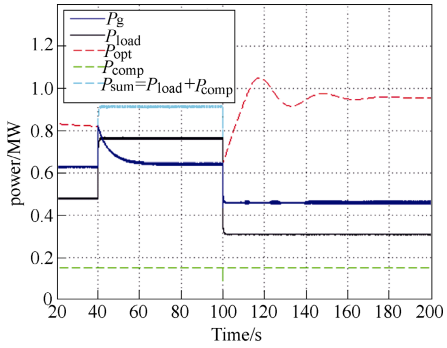

(h) Wind turbine power

Fig.11 The performance of the system for step change of load

When wind speed is stepped down at 40s, the wind turbine torque is decreased, and the optimal power P_{opt} is reduced along with the decrease of the wind turbine speed. Until 47s, the power P_{opt} is less than the sum power P_{sum}, the generator operation follows the optimal power P_{opt}. Here, the generator could not support the loads in this wind speed as 8 m/s. In order to keep the DC-link voltage constant, the BESS releases its power to provide the loads, which result in the decrease of SOC shown in Fig.12(g).

At 100s, the wind speed is stepped up to 11.5 m/s, when the wind turbine speed is increased by the increase of the wind turbine torque. Until 106.5 s, the optimal power P_{opt} is over the power P_{sum}. Here, the PMSG is operated following the power P_{sum} again. The BESS starts to absorb the generator power, which causes the increase of SOC shown in Fig.12(g). During operation, the pitch angle control is active to limit the wind turbine speed in Fig.12(c). As well, the DC-link voltage V_{dc} is nearly kept constant as illustrated in Fig.12(e).

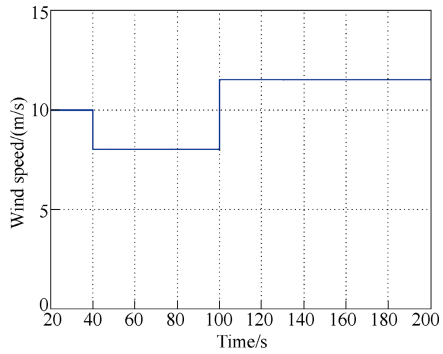

(a) Wind speed

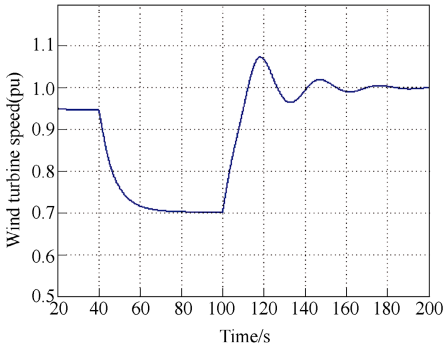

(b) Wind turbine speed

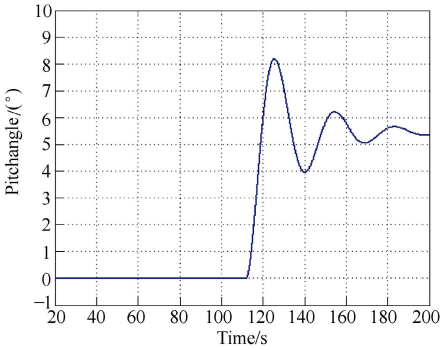

(c) Pitch angle

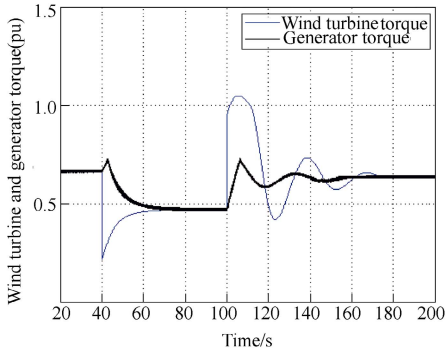

(d) Wind turbine torque and generator torque angle

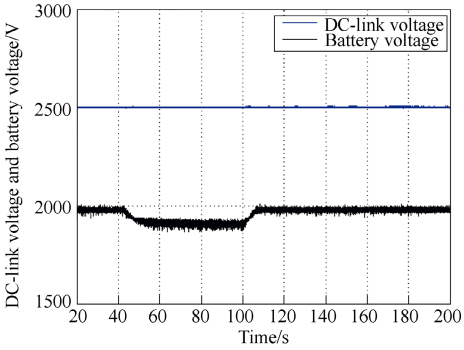

(e) DC-link voltage and battery voltage

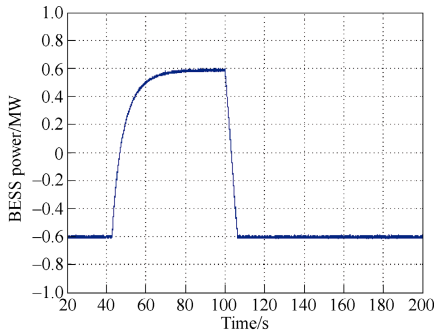

(f) BESS power

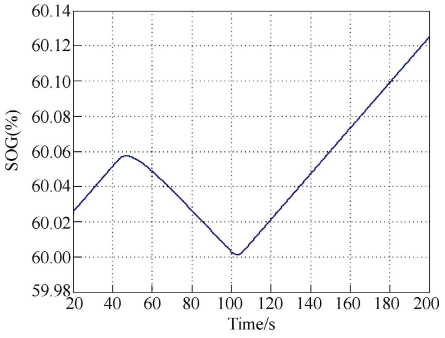

(g) SOC of battery

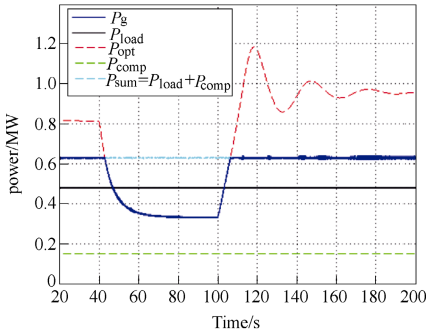

(h) Wind turbine power

Fig.12 The performance of the system for step change of wind speed

5.3 The third case

The performance of the stand-alone wind turbine system is tested in the third case, with the variable wind speed and loads in Fig.13(a) and (g). The DC-link voltage is kept almost constant in Fig.13(d), which ensures the normal operation of the wind turbine.

The ESS provides and absorbs the power in the wind turbine system, which could be shown from the power and energy change shown in Fig.13(e) and (f). The generator power P_g, loads power P_{load}, optimal power P_{opt} and P_{sum} are shown in Fig.13(g), which complies with the proposed operational principle.

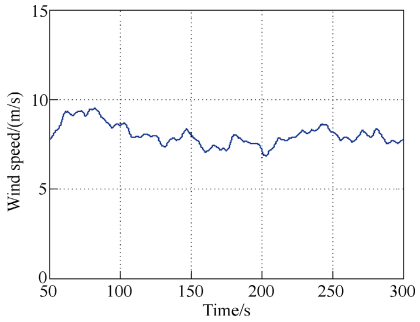

(a) Wind speed

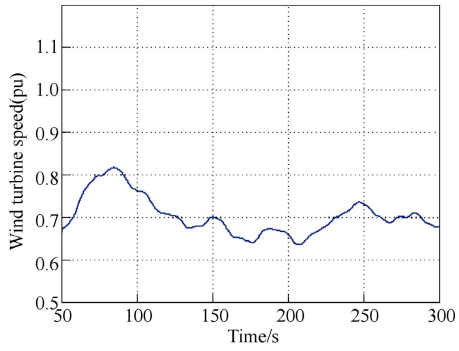

(b) Wind turbine speed

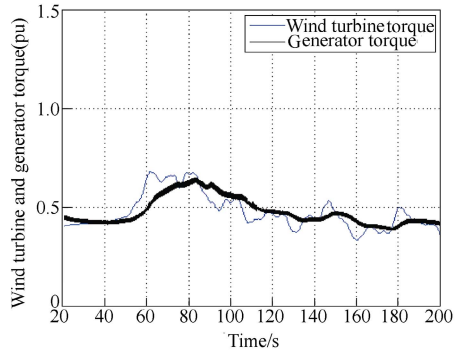

(c) Pitch angle

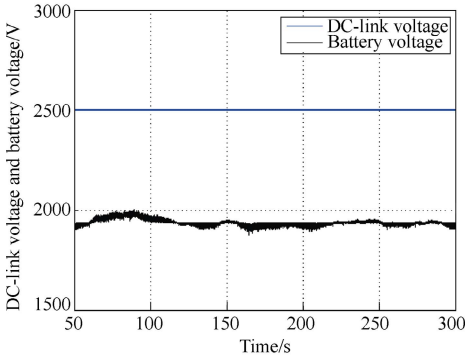

(d) DC-link voltage and battery voltage

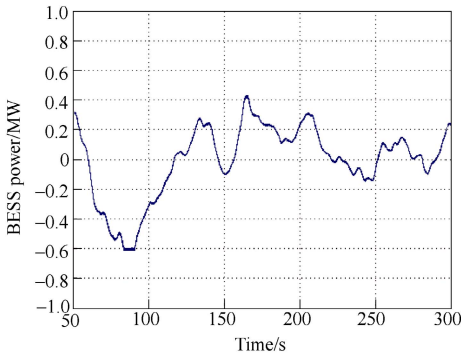

(e) BESS power

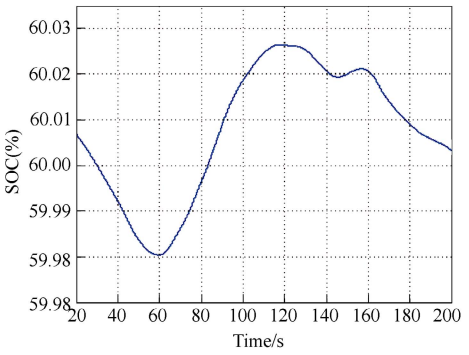

(f) SOC of battery

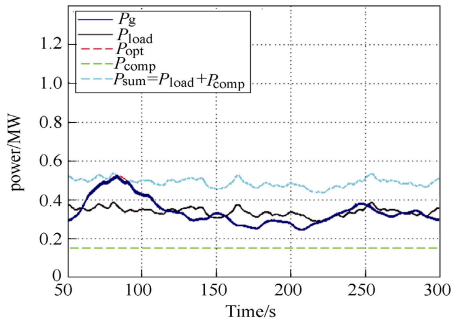

(g) Wind turbine power

Fig.13 The performance of the stand-alone wind turbine system

6 Conclusion

A stand-alone variable speed wind turbine based on PMSG, full-scale power converter and ESS has been presented in this paper. A novel control strategy for this stand-alone wind turbine system is proposed. The load-side converter is controlled using vector-control scheme to maintain the amplitude and frequency of the converter output voltage. The ESS has the bidirectional power control ability, which is used to keep the DC-link voltage of the full-scale power converter constant. At the same time, the generator-side converter operates together with the ESS to support the loads. The variable speed wind turbine with the proposed control strategy is suitable for a small-scale stand-alone generation system installation for remote-area power supply. A 4MW generation system based on the presented variable speed wind turbine is developed using PSCAD/EMTDC. The simulation results show that its ability to meet the operational needs of a variable speed wind turbine in a stand-alone system. It is feasible to meet the demand of the loads and wind speed variation. As well, it is capably of limiting the DC-link voltage of the full-scale power converter in a small rang so as to ensure the normal operation of the power electronics. Finally, it is concluded that the presented variable speed wind turbine and the proposed control strategy can be an effective solution to achieve power supply in a small-scale stand-alone generation system.

Appendix I

Table 2 Wind turbine and generator characteristic

Parameters	Value
Wind turbine rated power/MW	4
Rotor diameter/m	110
Rotating speed/ (r/m)	6.7~15
Nominal wind speed/ (m/s)	11.4
Generator rated power/MW	4
Stator rated line voltage /kV	1
Rated frequency/Hz	20
Number of pole pairs	88
Stator winding resistance (p.u.)	0.008
Windings leakage reactance X_l (p.u.)	0.06
d-axis reactance X_d (p.u.)	0.8
q-axis reactance X_q (p.u.)	0.5
Magnetic strength (p.u.)	1.2
Generator inertia/s	0.8
Equivalent wind turbine inertia/s	5.5
Shaft stiffness K (p.u.)	2.7
Shaft damping D (p.u.)	0.019

Table 3 Power converter and ECS characteristic

Parameters	Value
Capacitor C /F	0.08
Induction L_f /H	0.0001
Resistance R_f /Ω	0.0003
Induction L_s/H	0.001

Table 4 Control design parameters

Controller		K_p	T_i
BESS	Voltage controller	10	0.05
	Current controller	10	0.0025
Generator side	Voltage controller	1	0.02
	Power controller	0.05	0.008
	Current controller	0.2	0.2
Load side	Power controller	10	0.002
	Current controller	0.06	0.16

Appendix II

Table 5 Characteristics of energy storage system

Storage system	Specific energy cost c_e/(k€/MWh)	Special power cost c_p/(k€/MWh)	M & O m (%)
Lead acid battery	210	140	1
FC	10	300	1

Appendix III

Fig.5 shows the battery model, which is detailed illustrated in[34]. Only the main parts are introduced briefly in this appendix. The SOC and DOC of the battery are defined as

$$\begin{cases} \text{SOC} = 1 - \dfrac{Q_e}{K_c C_{0^*}} \\ \text{DOC} = 1 - \dfrac{Q_e}{K_c C(I_{avg}, \theta)} \end{cases} \tag{A.1}$$

with

$$Q_e(t) = \int_0^t -i_{\text{m}}(\tau)\,\text{d}\tau \tag{A.2}$$

$$C(I,\theta) = \frac{K_c C_{0^*}(1-\theta/\theta_f)^{\varepsilon}}{1+(K_c-1)(I/I^*)^{\delta}} \tag{A.3}$$

The electrolyte temperature θ is determined by the following differential equation

$$C_\theta \frac{\text{d}\theta}{\text{d}t} = P_{\text{s}} - \frac{\theta - \theta_a}{R_\theta} \tag{A.4}$$

with

$$P_{\text{s}} = I_{\text{m}}^2 (R_0 + R_2) \tag{A.5}$$

After SOC, DOC and θ are obtained, the battery parameters E_{m}, R_0, R_1, R_2, C_1 and parasitic branch current I_{p} can be determined by

$$\begin{cases} E_m = E_{m0} - K_E(273+\theta)(1-\text{SOC}) \\ R_0 = R_{00}\left[1 + A_0(1-\text{SOC})\right] \\ R_1 = -R_{10}\ln(\text{DOC}) \\ R_2 = -R_{20}\dfrac{\exp\left[A_{21}(1-\text{SOC})\right]}{1+\exp(A_{22}I_m/I^*)} \\ C_1 = \tau/R_1 \\ I_{\text{p}} = V_{\text{PN}} G_{\text{p0}} \exp\left[V_{\text{PN}}/V_{\text{p0}} + A_{\text{p}}(1-\theta/\theta_{\text{f}})\right] \end{cases} \tag{A.6}$$

where E_{m0}, K_{E}, R_{00}, A_0, R_{10}, R_{20}, A_{21} and A_{22} are constants for the specific battery and could be obtained by experimental method.

Appendix IV

The parametric values of each battery cell [34] are as follows:

I^*=49A, C_{0^*}=261.9Ah, K_c=1.18, θ_f=−40℃, ε=1.29, δ=1.4, τ=5000s, E_{m0}=2.135 V, K_{E}=0.00058V/℃, R_{00}=2mΩ, R_{10}=0.7mΩ, R_{20}=15mΩ, A_0=−0.3, A_{21}=−8, A_{22}=−8.45, E_{p}=1.95V, V_{p0}=0.1V, G_{p0}=2 ps, A_{p}=2, C_θ=15 Wh/℃, R_θ=0.2℃/W.

References

[1] Z. Chen, Y. Hu, and F. Blaabjerg, "Stability improvement of induction generator-based wind turbine systems," *IET Renewable Power Generation,* vol. 1, pp. 81-93, March 2007.

[2] S. M. Muyeen, R. Takahashi, T. Murata, and J. Tamura "A variable speed wind turbine control strategy to meet wind farm grid code requirements," *IEEE Trans. Power System*, vol. 25, no. 1, pp. 331-340, Jan. 2010.

[3] R. Zhu, Z. Chen, X. Wu, and F. Deng, "Virtual damping flux based LVRT control for DFIG-based wind turbine," *IEEE Trans. Energy Convers.*, vol.30, no.2, pp.714-725, Jun. 2015.

[4] S. Abulanwar, W. Hu, Z. Chen, and F. Iov, "Adaptive voltage control strategy for variable-speed wind turbine connected to a weak network," *IET Renewable Power Generation*, vol. 10, no. 2, pp. 238-249, Feb. 2016.

[5] J. G. Slootweg, S. W. H. de Haan, H. Polinder, and W. L. Kling, "Aggregated modelling of wind parks with variable speed wind turbines in power system dynamics simulations," *in Proc. IEEE Power Tech. Conf.*, Bologna, 2003, pp. 1-6.

[6] F. Huerta, R. Tello, and M. Prodanovic, "Real-time power-hardware-in-the-loop implementation of variable-speed wind turbines," *IEEE Trans. on Ind. Electron.*, vol. 64, no. 3, pp. 1893-1904, Mar. 2017.

[7] M. E. Haque, M. Negnevitsky, and K. M. Muttaqi, "A novel control strategy for a variable-speed wind turbine with a permanent-magnet synchronous generator," *IEEE Trans. on Ind. Appl.*, vol. 46, no. 1, pp. 331-339, Jan./Feb. 2010.

[8] Y. Kim, M. Kang, E. Muljadi, J. Park, and Y. Kang, "Power smoothing of a variable-speed wind turbine generator in association with the rotor speed–dependent gain," *IEEE Trans. Sustainable Energy*, vol. PP, no. 99, pp. 1-1, Dec. 2016.

[9] H. Li, and Z. Chen, "Overview of different wind generator systems and their comparisons," *IET Renewable Power Generation*, vol. 2, no. 2, pp.123-138, Jun. 2008.

[10] Zhe Chen, J. M. Guerrero, and F. Blaabjerg, "A review of the state of the art of power electronics for wind turbines," *IEEE Trans. Power Electron.*, vol. 24, no. 8, pp. 1859-1875, Aug. 2009.

[11] M. Chinchila, S. Arnaltes, and J. C. Burgos, "Control of permanent-magnet generators applied to variable-speed wind-energy systems connected to the grid," *IEEE Trans. Energy Convers.*, vol. 21, no. 1, pp. 130-135, Mar. 2006.

[12] R. Rathnayake, R. Dutta, J. Fletcher, "Control of direct driven fractional slot concentrated wound-IPMSG for variable speed wind energy system," in *Proc. IEEE ICEM*, Suntec, 2016, pp. 1001-1007.

[13] X. Yuan, F. Wang, D. Boroyevich, Y. Li, and R. Burgos, "DC-link voltage control of a full power converter for wind generator operating in weak-grid systems," *IEEE Trans. Power Electron.*, vol. 24, no. 9, pp. 2178-2192, Sep. 2009.

[14] M. Davari, and Y. Mohamed, "Robust DC-link voltage control of a full-scale PMSG wind turbine for effective integration in DC grids," *IEEE Trans. Power Electron.*, vol. 32, no. 5, pp. 4021-4035, May 2017.

[15] A. Kassem, and S. Zaid, "Load parameter waveforms improvement of a stand-alone wind-based energy storage system and Takagi-Sugeno fuzzy logic algorithm," *IET Renewable Power Generation*, vol. 8, no. 7, pp. 775-785, 2014.

[16] Y. Zuo, and X. Li, "Game theory applied in system of renewable power generation with HVDC out-sending facilitated by hundred megawatts battery energy storage station," in *Proc. IEEE SSCI*, Athens, 2016, pp. 1-5.

[17] J. P. Barton and D. G. Infield, "Energy storage and its use with intermittent renewable energy," *IEEE Trans. Energy Convers.*, vol. 19, no. 2, pp. 441-448, Jun. 2004.
[18] C. Nguyen, and H. Lee, "Optimization of power dispatch to minimize battery storage capacity in wind farm," in *Proc. IEEE ECCE*, Pittsburgh, 2014, pp. 420-427.
[19] X. Y. Wang, D. Mahinda Vilathgamuwa, and S. S. Choi, "Determination of battery storage capacity in energy buffer for wind farm," *IEEE Trans. Energy Convers.*, vol. 23, no. 3, pp.868-878, Sep. 2008.
[20] Wang Caisheng, and M. H. Nehrir, "Power management of a stand-alone wind/photovoltaic/fuel cell energy system," *IEEE Trans. Energy Convers.*, vol. 23, no. 3, pp. 957-967, Sep. 2008.
[21] Energinet. DK, http://www.energinet.dk/en/menu/Market/Download+of+Market+Data/Download+of+Market+Data.htm.
[22] P. Thounthong, V. Chunkag, P. Sethakul, B. Davat, and M. Hinaje, "Comparative study of fuel-cell vehicle hybridization with battery or supercapacitor storage device," *IEEE Trans. Veh. Techn.*, vol. 58, no. 8, pp. 3892-3904, Oct. 2009.
[23] J. K. Kaldellis, D. Zafirakis, and K. Kavadias, "Techno-economic comparison of energy storage systems for island autonomous electrical networks," *Renewable and Sustainable Energy Reviews*, vol. 13, no. 2, pp. 378-392, Feb. 2009.
[24] Tao Sun, Zhe Chen, and Frede Blaabjerg, "Transient stability of DFIG wind turbines at an external short-circuit fault," *Wind Energy*. vol. 8, no. 3, pp.345-360, Aug. 2005
[25] X. Wang, and D. Sun, "Three-vector-based low-complexity model predictive direct power control strategy for doubly fed induction generators," *IEEE Trans. Power Electron.*, vol. 32, no.1, pp.773-782, Feb. 2016.
[26] S. Xie, M. Li, H. Li, J. Luo, and C. Zhao, "Maximum power point tracking control strategy for variable speed wind turbine generation system," in *Proc. ISEEE*, Sapporo, 2014, pp. 1-8.
[27] Tao Sun, Zhe Chen, and F. Blaabjerg, "Flicker study on variable speed wind turbines with doubly fed induction generators," *IEEE Trans. Energy Convers.*, vol. 20, no. 4, pp.896-905, Dec. 2005.
[28] E. Muljadi, and C. P. Butter field, "Pitch-controlled variable-speed wind turbine generation," *IEEE Trans. Ind. Appl.,* vol. 37, no. 1, pp. 240-246, Jan./Feb. 2001.
[29] Y. Zhang, Z. Chen, W. Hu, and M. Cheng, "Flicker mitigation by individual pitch control of variable speed wind turbines with DFIG," *IEEE Trans. Energy Convers.*, vol. 29, no. 1, pp. 20-28, Mar. 2014.
[30] Fujin Deng, and Zhe Chen, "Power control of permanent magnet generator based variable speed wind turbines," *ICEMS 2009*, pp. 1-6.
[31] A. Patil, and A. Thosar, "Steady state and transient stability analysis of wind energy system," in *Proc. IEEE CIEC*, Kolkata, 2016, pp. 250-254.
[32] S. M. Muyeen, Md. Hasan, R. Takahashi, T. Murata, J. Tamura, Y. Tomaki, A. Sakahara, and E. Sasano, "Comparative study on transient stability analysis of wind turbine generator system using different drive train models," *IET Renew. Power Gener.*, vol. 1, no. 2, pp. 131-141,2017.
[33] S. Barsali, and M. Ceraolo, "Dynamic models of lead-acid batteries: Implementation issues," *IEEE Trans. Energy Convers.*, vol. 17, no. 1, pp. 16-23, Mar. 2002.
[34] M. Ceraolo, "New dynamical models of lead-acid batteries," *IEEE Trans. Power System*, vol. 15, no. 4, pp. 1184-1190, Nov. 2000.
[35] T. Morstyn, A. Savkin, B. Hredzak, and V. Agelidis, "Multi-agent sliding mode control for state of charge balancing between battery energy storage systems distributed in a DC microgrid," *IEEE Trans. Smart Grid*, Accepted, 2017.
[36] S. Teleke, M. E. Baran, S. Bhattacharya, and A. Q. Huang, "Control strategies for battery energy storage for wind farm dispatching," *IEEE Trans. Energy Convers*, vol. 24, no. 3, pp. 725-732, Sep. 2009.
[37] J. G. Slootweg, S. W. H. de Haan, H. Polinder, and W. L. Kling, "General model for representing variable speed wind turbines in power system dynamics simulations," *IEEE Trans. Power System*, vol. 18, pp. 144-151, Feb. 2003.
[38] Gene F. Franklin, and J. David Powell, *Feedback Control of Dynamic Systems* (4th Edition), New Jersey: Prentice Hall, 2002.

Fujin Deng received the B. Eng. degree in electrical engineering from China University of Mining and Technology, Jiangsu, China, in 2005, the M. Sc. Degree in electrical engineering from Shanghai Jiao Tong University, Shanghai, China, in 2008, and the Ph. D. degree in energy technology from the Department of Energy Technology, Aalborg University, Aalborg, Denmark, in 2012.

From 2013 to 2015, he was a Postdoctoral Researcher with the Department of Energy Technology, Aalborg University, Aalborg, Denmark. From 2015 to 2017, he was an Assistant Professor with the Department of Energy Technology, Aalborg University, Aalborg, Denmark. Since 2017, he joined the School of Electrical Engineering, Southeast University, China, as a Professor. His research interests include wind power generation, high-power conversion, power electronics, DC grid, high-voltage direct-current(HVDC) technology, and offshore wind farm-power systems dynamics.

Dong Liu received the B.Eng. degree and M.Sc. degree in electrical engineering from South China University of Technology, Guangdong, China, in 2008 and 2011 respectively. He is currently working toward the Ph. D. degree in the Department of Energy Technology, Aalborg University, Denmark.

From 2011 to 2014, he was a R&D Engineer in Emerson Network Power Co., Ltd., Shenzhen, China. His main research interests include renewable energy technology, multilevel converters, and DC/DC converters.

Zhe Chen received the B. Eng. and M. Sc. degrees from the Northeast China Institute of Electric Power Engineering, Jilin, China, and the Ph.D. degree from University of Durham, U.K.

He is a full Professor with the Department of Energy Technology, Aalborg University, Aalborg, Denmark. He is the Leader of Wind Power System Research Program at the Department of Energy Technology, Aalborg University, and the Danish Principle Investigator for *Wind Energy* of *Sino-Danish Centre for Education and Research*. He has led many research projects and has more than 360 publications in his technical field. His research areas are power systems, power electronics, and electric machines, and his main current research interests include wind energy and modern power systems.

Dr Chen is an Editor of the IEEE Transactions on Power Systems, an Associate Editor (Renewable Energy) of the IEEE Transactions on Power Electronics, a Fellow of the Institution of Engineering and Technology (London, U.K.), and a Chartered Engineer in the U.K.

Peng Su was born in Henan, China, in 1988. He received the B. Sc. and M. E. degrees in electrical engineering from Henan Polytechnic University, Henan, China in 2011 and 2013, respectively. Since 2013, he has been with the School of Electrical Engineering, Southeast University, Nanjing, China, where he is currently working toward the Ph.D. degree.

His current research interests include the design and analysis of novel permanent-magnet brushless electrical machines for application in electric vehicles.